ionic conduction of the simulated borosilicate glasses was 1.38-1.45 eV in the high temperature region (500-620 °C, 420-620 °C, 392-620 °C, 368-620 °C for SW, SWFP2, SWFP5, SWFP10, respectively) and 0.93-1.1 eV in the low temperature region (150-480 °C, 150-410 °C, 150-388 °C, 130-360 °C, for SW, SWFP2, SWFP5, SWFP10, respectively).

## References

1. West, H. R. *Solid State Chemistry and its Applications*; John Wiley & Sons: New York, U. S. A., 1984; p 452.
2. White, W. B. In *Corrosion of Glass, Ceramic and Ceramic Superconductor*; Clark, D. E.; Zoitos, B. K., Ed.; Noyes Publ.: Park Ridge, New Jersey, U. S. A., 1992; p 21.
3. Douglas, R. W.; Israd, J. O. *J. Soc. Glass Technol.* **1949**, *33*, 289.
4. Rawson, H. *Properties and Applications of Glass*; Elsevier: Netherlands, 1980; p 247.
5. Cunnane, J. C.; Bates, J. K.; Ebert, W. L.; Feng, X.; Mazer, J. J.; Wronkiewicz, D. J.; Sproull, J.; Boucier, W. L.; McGrail, B. P. *Mat. Res. Soc. Symp. Proc.* **1993**, *294*, 225.
6. US Department of Energy Report, *Defense Waste Processing Facility: Savannah River Plant, Aiken, SC. Final environmental impact statement*, DOE/EIS-0082, 1982.
7. Nogues, J. L.; Vernaz, E. Y.; Jacquet-Francillon, N. *Mat. Res. Soc. Symp. Proc.* **1985**, *44*, 89.

# Local Structure Refinement of the $BaFe_{1-x}Sn_xO_{3-y}$ System with Fe K-Edge X-Ray Absorption (XANES/EXAFS) Spectroscopy

**Min Gyu Kim, Ki Seop Kwack, Kwon Sun Roh, and Chul Hyun Yo***

*Department of Chemistry, Yonsei University, Seoul 120-749, Korea*
*Received April 7, 1997*

Local structure refinement of the $BaFe_{1-x}Sn_xO_{3-y}$ system ($x$=0.00-0.50) has been carried out with Fe K-edge x-ray absorption spectroscopic studies. It is found out that the Fe ions are placed in two different symmetric sites such as tetrahedral and octahedral sites in the compounds by comparison with Fe K-edge x-ray absorption near edge structure (XANES) spectrum of the $\gamma$-$Fe_2O_3$ compound as a reference. Small absorption peaks of dipole-forbiden transitions appear at a pre-edge region of 7111 eV due to the existence of Fe ions in the tetrahedral and octahedral sites. The peak intensity decreases with the substitution amount of Sn ion. Three different absorption peaks of 1s→4p dipole-allowed transition appear on the energy region between 7123 and 7131 eV. The peaks correspond to 1s→4p main transition of Fe ions in tetrahedral and octahedral sites and 1s→4p transition followed by the shakedown process of ligand to metal charge transfer. The bond distances between Fe ions in the tetrahedral site and nearest neighboring oxygen atom (Fe-4O), and those in octahedral site (Fe-6O) are determined with the extended x-ray absorption fine structure (EXAFS) analysis. Two different interatomic distances increase with the substitution amount of Sn ion and also the bond lengths of Fe-4O are shorter than those of Fe-6O in all compounds.

## Introduction

The physical properties of perovskite-related metal oxides have been related closely to their structures. A number of studies for the transition metal oxides have been carried out extensively with various analytical methods in order to find relationships between their structures and physical properties. In general, physical properties such as electrical conductivity and magnetic susceptibility depend on the bonding character between transition metal and oxygen ions as well as the degree of local structural distortion on the transition metal elements.[1-5] Accurate structural refinement of compounds is important for the characterization of metal oxides.

Generally, oxygen nonstoichiometric perovskite-type oxides include both tetrahedral and octahedral sites for an atom. Therefore, it is difficult to determine the distance between each atomic site and ligand atom to molecular dimension scale with XRD since the atomic sites distribute randomly in the compounds. However, X-ray absorption spectroscopy is useful for structural analysis of the nonstoichiometric compounds since it is very specific to atomic local sites

Structural analysis of X-ray absorption (XANES/EXAFS) spectroscopy is used for local struture refinement on an interesting ion. For XANES (x-ray absorption near edge structure) spectroscopy, the spectra can result from the transition of a core electron to bound states. Therefore x-ray absorption pre-edge features give useful informations such as the oxidation state of chemical species, site symmetry of x-ray absobing atom, and covalency. The dipole selection rules ($\Delta l = \pm 1$) can be applied to the x-ray absorption spectroscopy, and the x-ray absorption occurs under an electron transition approximation. The dipole matrix element between an intial core state $|i\rangle$ and a final state $|f\rangle$ is fol-

lowed,

$$\sigma_{abs}(E)=\frac{4\pi^2e^2}{\hbar c}E|<f|e\cdot r|i>|^2,$$

where σis the x-ray absorption cross section, $E$ is the photon energy, and $e$ is an unit vector in the direction of the electric field.[6-10]

In general, a small pre-edge peak of the K-edge absorption spectra for transition metal compounds with partially filled d orbitals has been assigned to the transition from *1s* to *nd* orbitals even though it is dipole-forbidden transition. The transition has different intensities between tetrahedral and octahedral atomic sites and thus has been used to infer a site symmetry in transition metal compounds.[11-15] Some molecular orbital calculation studies have been reported that the pre-edge spectra of Fe compounds show a small absorption peak assigned to the transition from *1s* to *nd*, which might be related with the Fe *3d* and *4p* orbital mixing and with the site symmetry.[16,17] They have shown that the pre-edge intensity generally increases with the departure from centrosymmetric coordination environment. Namely, the pre-edge absorption intensity increase from octahedral, five-coodinate to tetrahedral sites in turn. The EXAFS (extended x-ray absorption fine structure) spectra have provided many quantatitive characterizations such as the bond length, coordination number on absorbing atom, and the Debye-Waller factor etc.[18-20] The EXAFS spectroscopy is powerful for the structural analysis because it is very sensitive to local site of x-ray absorbing atom.

In the present study, the local structural refinement around Fe ions in the tetrahedral and octahedral sites for the nonstoichiometric $BaFe_{1-x}Sn_xO_{3-y}$ (x=0.00, 0.25, and 0.50) system has been studied with the spectroscopic analysis.

## Experimental

**Synthesis and Chemical Analysis.** Oxygen nonstoichiometric compounds of the $BaFe_{1-x}Sn_xO_{3-y}$ system have been prepared by ceramic method with appropriate stoichiometric starting materials such as all spectroscopic pure $BaCO_3$, $SnO_2$, and $Fe_2O_3$ powders. The mixtures are prefired at 900 °C for 6 hours under the air atmosphere. Pelleting under a pressure of 3.0 ton/cm$^2$, heating at 1350 °C for 24 hours, and then quenching are followed. The grinding and heat treatment are repeated in order to prepare the homogeneous nonstoichiometric solid solutions. The homogeneous phase of each compound and the ratio of composition has been identified and verified by X-ray diffraction analysis with monochromatic Cu $K_\alpha$ (λ=0.15418 nm) and X-ray fluorescence (XRF) analysis, respectively. The mole ratio of the $Fe^{4+}$ ion to total Fe ion (τ) and the oxygen vacancies (y) could be determined by the potentiometric titration in which $I_2$ formed by reduction of both $Fe^{3+}$ and $Fe^{4+}$ ions to $Fe^{2+}$ ions in KI solution is titrated with standard sodium thiosulfate solution in nitrogen atmosphere in order to prevent $I_2$ to be oxidized.

**Fe K-edge XANES/EXAFS Measurement.** Fe K-edge X-ray absorption (XANES/EXAFS) spectra are recorded on the beam line 6B of Photon Factory with the ring current of 300~350 mA at National Laboratory for High Energy Physics in Japan. Si(111) monochromator crystal is used to record the XANES/EXAFS data. Energy calibrations have been carried out with the iron metal and iron oxide (γ-$Fe_2O_3$) powder. The data are collected in a transmittance mode with the nitrogen (75%) and argon (25%) gases-filled ionization chambers as detectors. To record the XANES spectra for the electronic transition to bound states accurately, the data are taken with $\Delta E/E\sim2\times10^{-4}$ for BL6B in the XANES region.

**EXAFS Data Analysis.** The first consideration of EXAFS theory corresponds to single scattering of a photoelectron which has enough kinetic energy. The EXAFS spectra can be obtained due to a final state interference effect between an outgoing photoelectron wave from the x-ray absorbing atom and an incoming wave scattered from neighboring atoms. The single sacattering process gives rise to an oscillatory x-ray absorption rate or μ(E). After the removal of the background absorption or $\mu_o$(E), the x-ray absorption rate is normalized with respect to the background absorption. Then the normalized EXAFS oscillation can be expressed as follows:

$$\chi(k)=\frac{\mu(E)-\mu_o(E)}{\mu_o(E)}=\sum N_j S_o^2F_j(k)\exp(-2\sigma_j^2k^2)$$
$$\exp(-2r_j/\lambda_j(k))\frac{\sin(2kr_j+\Phi_{ij}(k))}{kr_j^2}$$

where includes photoelectron wave vector, $k$(=$[2m(E-E_o)/\hbar^2]^{1/2}$), coordination number, $N_j$, effective curved wave backscattering amplitude, $f_j(\pi)$, many body amplitude reduction factor, $S_o^2$, the Debye-Waller factor, $\sigma_j^2$, the mean free path of the photoelectron, λ, the interatomic distance $R_j$, and total phase shift $\Phi_{ij}$.

These structural parameters can be determined by the comparison with an experimental and a theoretical reference compound.[21,22] The theoretical single scattering paths on the Fe atom in two γ-$Fe_2O_3$ and $LaSrFeSnO_6$ model compounds are determinded with FEFF6.01 code. The $k^3$-weighted χ(k) signals Fourier filtered in the interesting FT region with the hanning window function could be fitted by nonlinear fit of each scattering path in the $k$ region between 20 and 140 nm$^{-1}$ with FEFFIT code. In the fitting process of filtered experimental EXAFS spectra, a relative goodness-of-fit parameter is given in the forn of a normalized $\chi^2$ value, calculated acoording to

$$\chi^2=\frac{N_{idp}}{N}\sum_{i=1}^{N}[(\chi_{data}-\chi_{model})/\varepsilon_i]^2$$

where $N_{idp}$ is the number of independent data points, $N$ is the number of experimental data points, $\chi_{data}$-$\chi_{model}$ is the difference between the experimental data and the calculated fit for each point $i$, and $\varepsilon_i$ is the uncertainty in the measurement, respectively.

## Results and Discussion

**Fe K-edge XANES spectroscopy.** Fe K-edge XANES (x-ray absorption near edge structure) spectra of the $BaFe_{1-x}Sn_xO_{3-y}$ system (x=0.00-0.50) are shown in Figure 1. In order to present the detailed features in the absorption edges, second derivatives of the spectra could be obtained after the recorded spectra are subtracted with the arctangent

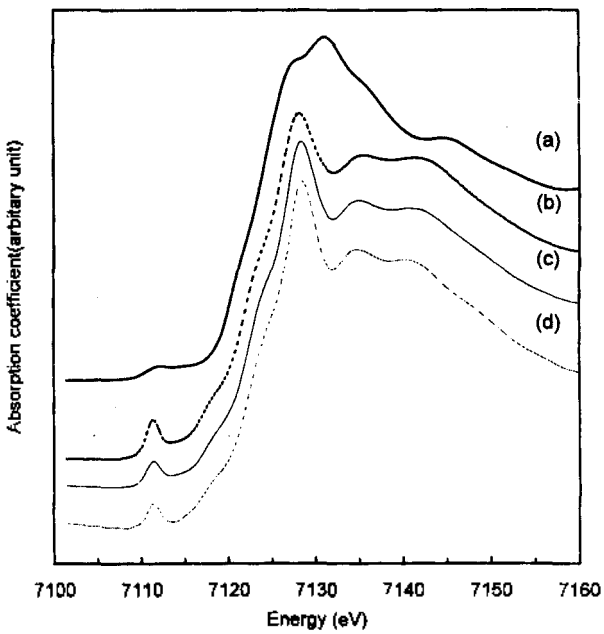


**Figure 1.** Normalized Fe K-edge XANES spectra for (a) $\gamma$-$Fe_2O_3$, (b) $BaFeO_{2.61}$, (c) $BaSn_{0.25}Fe_{0.75}O_{2.65}$, and (d) $BaSn_{0.50}Fe_{0.50}O_{2.76}$ compounds.

curves which approximates the transition of the core electron to continuum states as shown in Figure 2. Table 1 shows the Lorentzian-fitting parameters for second derivatives of the Fe K-edge XANES spectra. The peaks of the second derivatives are fitted with the Lorentzian curves in order to determine accurate energy positions corresponding to the core electron transition to bound states.

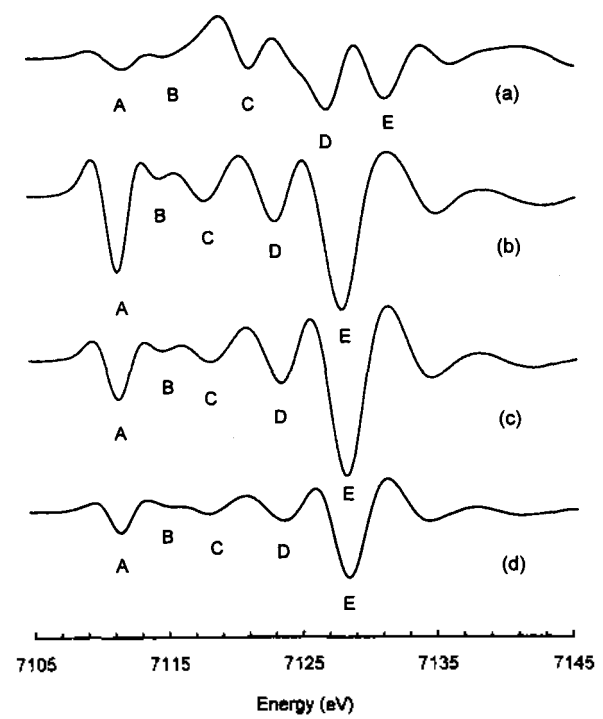


**Figure 2.** Second derivaives of normalized Fe K-edge XANES spectra for (a) $\gamma$-$Fe_2O_3$, (b) $BaFeO_{2.61}$, (c) $BaSn_{0.25}Fe_{0.75}O_{2.65}$, and (d) $BaSn_{0.50}Fe_{0.50}O_{2.76}$ compounds.

**Table 1.** Peak positions for core electron transitions from second derivatives of Fe K-edge XANES spectra for the $BaFe_{1-x}Sn_xO_{3-y}$ system determined by Lorentzian curve fitting*

| Compound | Peak position (E/eV) | | | | |
|---|---|---|---|---|---|
| | A[1] | B[2] | C[3] | D[4] | E[5] |
| $\gamma$-$Fe_2O_3$ | 7111.8 | ~7115.0 | 7121.3 | 7126.9 | 7131.3 |
| x=0.00 | 7111.3 | 7114.4 | 7117.9 | 7123.1 | 7128.0 |
| x=0.25 | 7111.3 | 7114.6 | 7118.2 | 7123.5 | 7128.3 |
| x=0.50 | 7111.5 | 7115.3 | 7118.2 | 7123.6 | 7128.5 |

*The peaks are fitted with the Lorentzian function, $f(E)=2A\Gamma/\Pi\{\Gamma^2+4(E-E_c)^2\}$, where E, A, and $\Gamma$ represent peak position, peak area, and full width at half maximum of the peak, respectively.[1] 1s→3d transition allowed by quadrupole allowed transition. [2,3]Dipole-allowed 1s→4p transitions followed by the shakedown process of ligand to metal charge transfer (LMCT). [4,5]Dipole-allowed 1s→4p main transitions by dipole matrix approximation.

All compounds have shown small absorption peaks at the pre-edge region of about 7111 eV. The peak absorption is relatively small and broad for the $\gamma$-$Fe_2O_3$ reference compound as shown in Figure 1. It is well known that the $Fe^{3+}$ ions are filled in the tetrahedral (Td) and the octahedral (Oh) sites with the ratio of about 1 : 2 for the $\gamma$-$Fe_2O_3$ compound. The peak at the pre-edge region for the reference compound is ascribed to the $Fe^{3+}$ ions in the Td sites. Since the Fe ions in the Oh sites can keep the centrosymmetric environment rather than those in the Td sites, the Fe ion in the Oh sites shall not contribute to the small absorption peak.

The absorption peak at the pre-edge region results from a decrease of local symmetry on the x-ray absorbing atom and thus the peak intensity can inform the relative distribution of the Td sites through the compound. The peak intensity for the $BaFe_{1-x}Sn_xO_{3-y}$ system decreases as the substitution amount of the Sn ions increases. This trend shows that the relative distribution of Fe ions in the Td sites with respect to those in the Oh sites increases, which is in agreement with the the oxygen nonstoichiometry obtained from the chemical analysis. As shown in Table 2, the increase of positive charge produced by the substitution of Sn ions for Fe ions can be mainly compensated with the decrease of oxygen vacancies and then results in the increase of the Fe ion in octahedral sites.

The small peaks around 7111 eV of the Fe K-edge XANES spectra generally assign to 1s→3d transition which could not be expected with the electric dipole matrix. However, the forbidden 1s→3d pre-edge transition appears with small absorption of the electric quadrupole allowed transition. The peaks of the second derivatives could be des-

**Table 2.** The $\tau$ and $y$ values and nonstoichiometric chemical formula for the $BaFe_{1-x}Sn_xO_{3-y}$ system

| x value | $\tau$ value[a] | y value[b] | Nonstoichiometric chemical formula |
|---|---|---|---|
| 0.00 | 0.22 | 0.39 | $BaFe^{3+}_{0.78}Fe^{4+}_{0.22}O_{2.61}$ |
| 0.25 | 0.06 | 0.35 | $BaSn^{4+}_{0.25}Fe^{3+}_{0.69}Fe^{4+}_{0.06}O_{2.65}$ |
| 0.50 | 0.02 | 0.24 | $BaSn^{4+}_{0.50}Fe^{3+}_{0.48}Fe^{4+}_{0.02}O_{2.76}$ |

[a] Relative amount of $Fe^{4+}$ ion to total B site ions in the compounds. [b] Amount of oxygen vacancy.

cribed with the Lorentzian curves corresponding to the transitions to the bound states. Every single peaks for each compound are observed in similar line positions. Although an electron in the 1s core state can be excited to partially filled d orbitals or $t_{2g}$ and $e_g$ states, the spectra do not show the separation of two transitions to both $t_{2g}$ and $e_g$ states. The peak separation can not be observed under the small crystal field splitting of the Td site with this small absorption coefficient of the dipole forbidden transition.

The absorption peaks at the region between 7115 annd 7131 eV correspond to the dipole-allowed transition of 1s core electron to 4p energy level. The 1s→4p transition of a core electron and the creation of a core hole can produce two possible final states. The final states represent a $1s^1\underline{c}3d^5 4p^1$ electronic configuration of the main transition and a $1s^1\underline{c}3d^6\underline{L}4p^1$ configuration of shakedown process of ligand to metal charge transfer (LMCT), where $\underline{c}$ is a core hole and $\underline{L}$ is the ligand hole due to the LMCT process.

The peaks of 1s→4p main transition allowed by electric dipole matrix approximation appear in the energy region between 7123 and 7131 eV. The absorption coefficients of this transition are very strong due to the selection rule of $\Delta l$ =+1. The peaks in the region between 7115 and 7720 eV correspond to the 1s→4p main transition followed by the LMCT shakedown transition. These peaks appear in the lower energy region than only 1s→4p main peaks because the excited 1s→4p final state includes the relaxation process of valence levels due to the creation of a core hole. An increased effective nuclear charges with respect to the valence orbitals cause putting down the orbitals to lower energy levels, and then an electron from the O 2p orbitals can be transferred to 3d orbitals of the iron. Thus, the peaks are associated with the 1s→4p+LMCT shakedown transition.

In particular, it is interested in two different peaks with large absorption intensities at the region between 7128 and 7131 eV. In the γ-$Fe_2O_3$ and the $BaFe_{1-x}Sn_xO_{3-y}$ compounds, they might have simultaneously two x-ray absorbing elements such as Fe ions in the Td and Oh sites. The 1s→4p main transtions in two different Fe sites for the γ-$Fe_2O_3$ as reference compound are possible to occur at the different energy region. Grunes's study has shown for Fe K-edge absorption spectra of $Fe_2O_3$ compound that the 1s→4p transition occurs above 15.4 eV with respect to the 1s→3d dipole-forbidden transition. The large absorption peak above 18.4 eV from 1s→3d transition has been also assigned to the 1s→4p transition for the FeO compound with all Fe ions filled in the Oh sites.

For the present γ-$Fe_2O_3$ sample, two large absorption peaks are due to the 1s→4p transitions in the Td and Oh sites on the basis of Grunes's study.[8] These dipole-allowed transitions in two different absorbing elements have the energy difference of about 4 eV. The peaks corresponding to the 1s→4p transition for $BaFe_{1-x}Sn_xO_{3-y}$ compounds appear in the lower energy region than the γ-$Fe_2O_3$ compound. It is reasonable that the Td and Oh sites form the long range ordering in the γ-$Fe_2O_3$, while two sites form the short range ordering in the $BaFe_{1-x}Sn_xO_{3-y}$ compounds since the substituted Sn ions and oxygen vacancies can break site ordering.

**Fe K-edge EXAFS Spectroscopy.** The local atomic structures around x-ray absorbing atom in the $BaFe_{1-x}Sn_xO_{3-y}$ compounds have been determined quantatively by EXAFS spectroscopy. The γ-$Fe_2O_3$ compound with both Td and Oh sites of $Fe^{3+}$ ions is used as model compound. Since the present oxygen nonstoichiometric samples have Td and Oh sites simultaneously, the γ-$Fe_2O_3$ compound is suitable as a model compound in *ab initio* single scattering EXAFS calculation. The first shell of Fe ions is considered to two geometric environments of octahedrally coordinated Fe-6O and tetrahedrally coordinated Fe-4O with different interatomic distances. The interatomic distances of $Fe^{3+}$-6O (Oh) and $Fe^{3+}$-4O (Td) for the γ-$Fe_2O_3$ model compound are 0.2078 and 0.1889 nm from XRD, respectively.

Theoretical EXAFS parameters for the model compound such as phase shift, backscattering amplitude, and total central atom loss factor are calculated as a function of k for two single scattering paths, Fe-6O and Fe-4O by FEFF6.01 code, respectively. The values for amplitude reduction factor ($S_o^2$) and the debye-waller factor ($\sigma^2$) are not calculated in the ab initio calculation. For the simplicity in fitting process, $S_o^2$ will be fixed to the typical value of 0.85 for the Fe metal. Only two structural parameters for the debye-waller factor and interatomic distance can be used as adjustable parameters on the least square fitting process for the spectra of our samples.

The experimental Fe K-edge $k^3$-weighted EXAFS spectra for the γ-$Fe_2O_3$ and the $BaFe_{1-x}Sn_xO_{3-y}$ system are shown in Figure 3. Oscillatory signals for all Fe K-edge EXAFS spectra could be obtained after background removal and normalization processes with the threshold energy ($E_o$) of 7117.5 eV. Each signal is Fourier-transformated to the radial distribution function (RDF). Figure 4 shows two single scatterings by oxygen atoms coordinated around Fe atoms in Td

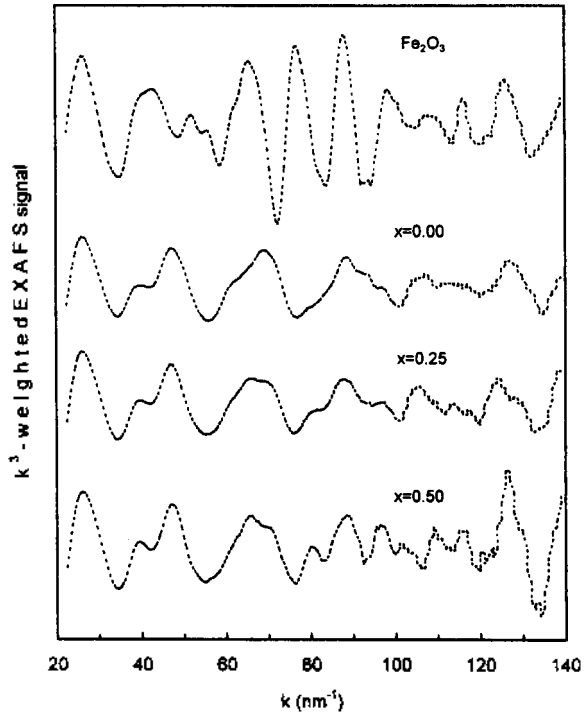


**Figure 3.** Experimental Fe K-edge EXAFS spectra obtained after background removal and normalization processes for (a) γ-$Fe_2O_3$, (b) $BaFeO_{2.61}$, (c) $BaSn_{0.25}Fe_{0.75}O_{2.65}$, and (d) $BaSn_{0.50}Fe_{0.50}O_{2.76}$ compounds.

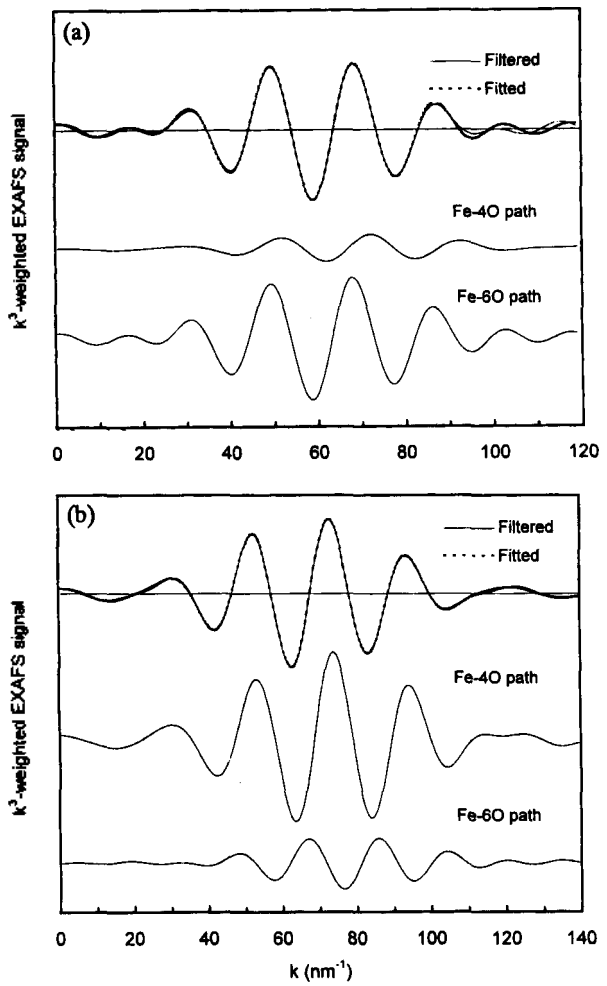


**Figure 4.** Experimental Fourier filtered (solid line) and fitted (dot line) EXAFS signals and each single scattering path for the first shells of Td (Fe-4O) and Oh (Fe-6O) sites, respectively. (a) $\gamma$-$Fe_2O_3$, (b) $BaFeO_{2.61}$ compounds.

and Oh sites for the $\gamma$-$Fe_2O_3$ and $BaFeO_{2.61}$ compounds. Two experimental scattering signals could be obtained with back Fourier-transformation in the RDF region between 0.12 and 0.23 nm for each RDF correspond to the single scattering for the first shells of Fe atoms in Td and Oh sites. The Fourier-filtered signals are fitted with two single scattering paths of *ab initio* EXAFS calculation from FEFF6.01 code. The result presents for the reference compound that the interatomic distances of Fe-4O and Fe-6O are 0.1899 and 0.2070 nm, respectively. The values are in good agteement with the reference values from XRD data.

**Table 3.** Structural parameters from EXAFS data analysis for the reference and $BaFeO_{2.61}$ compounds

| compound | Path | Structural parameters from EXAFS spectra | | | |
|---|---|---|---|---|---|
| | | $S_o^2$ | $E_o$ (eV) | R (Å) | $\sigma^2$ ($\times 10^{-3}$) |
| $\gamma$-$Fe_2O_3$ | Fe-4O | 0.85 | 1.2 | 1.89(9) | 10.4 |
| | Fe-6O | | -0.8 | 2.07(1) | 11.2 |
| $BaFeO_{2.61}$ | Fe-4O | 0.85 | 1.4 | 1.86(8) | 9.89 |
| | Fe-6O | | -2.1 | 2.03(5) | 10.1 |

Fitting process is carried out with fixed coordination number for each atom and 0.85 of $S_o^2$.

The local structures around the Fe ions for the $BaFeO_{2.61}$ compound can be determined with comparison to the structural results for $\gamma$-$Fe_2O_3$ compound. The oscillatory signals for the first shell could be obtained after Fourier-filtering of Fe K-edge EXAFS spectra for the oxygen nonstoichiometric compound similar to the case of the reference. For the simplicity in fit, The interatomic distance of $Fe^{4+}$-6O in the oxygen nonstoichiometric compound is approximated to be similar to that of $Fe^{3+}$-6O. The structural parameters are listed in Table 3 as the results of best fit for each filtered experimental signals with two calculated single scattering

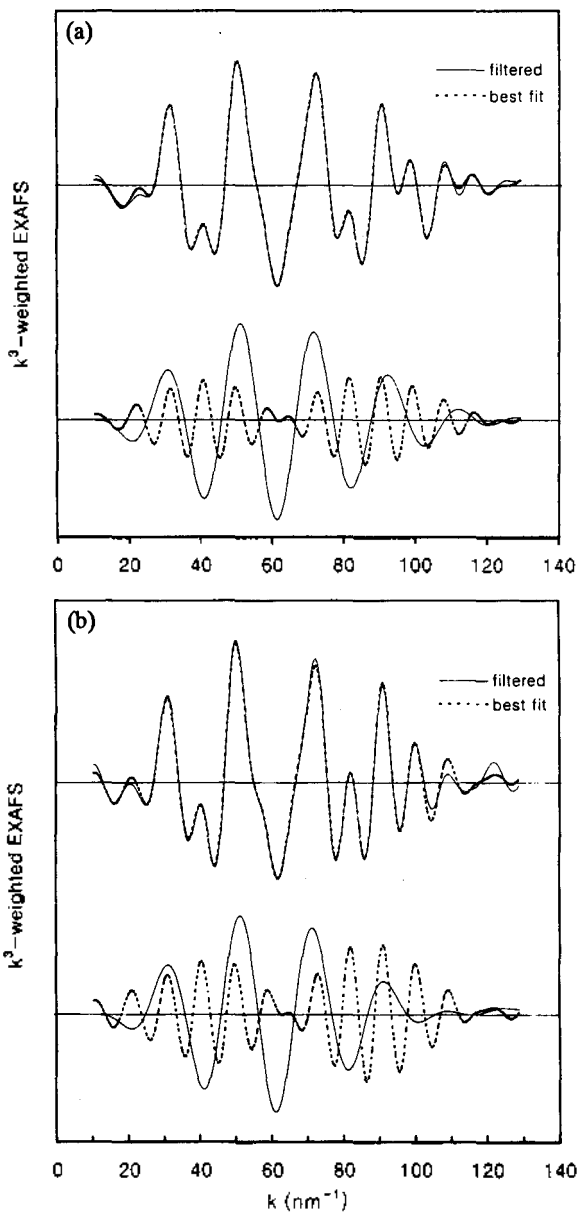


**Figure 5.** Experimental Fourier filtered (solid line) and fitted (dot line) EXAFS signals of total single scattering paths in FT region between 0.12 and 0.41 nm for $BaFe_{0.75}Sn_{0.25}O_{2.65}$ and $BaFe_{50}Sn_{0.50}O_{2.76}$ compounds. Two scattering paths by contribution of the first shell (solid line), the second and third shells (dot line) are shown in below figure.

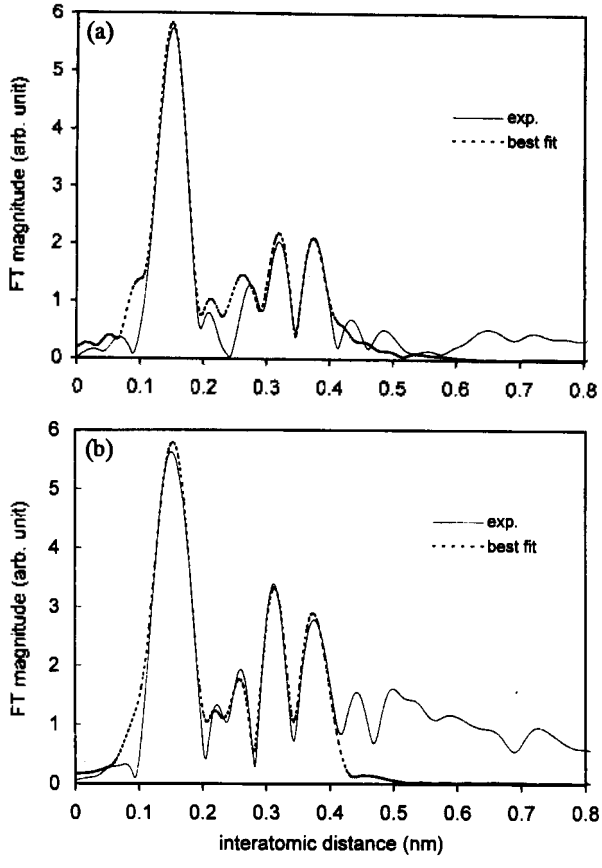


**Figure 6.** Fourier transformation magnitude of the partial radial distribution functions for raw experimental (solid line) and the fitted signals (dot line) of the $BaFe_{0.75}Sn_{0.25}O_{2.65}$ and $BaFe_{50}Sn_{0.50}O_{2.76}$ compounds.

paths.

Figure 5 shows the experimental Fourier filtered (solid line) and fitted (dot line) EXAFS signals of total single scattering paths for the first (Fe-4O and Fe-6O), second (Fe-Ba), and third (Fe-Fe/Sn) shells of $BaFe_{0.75}Sn_{0.25}O_{2.65}$ and $BaFe_{50}Sn_{0.50}O_{2.76}$ compounds. The Fourier transformation magnitude of the partial radial distribution functions for raw experimental (solid line) and the fitted signals (dot line) for all compounds are shown in Figure 6. In fitting processes, only three single scattering paths could be considered since a number of multiple scatterings are overlapped in ~0.4 nm FT region for the oxygen nonstoichiometric compounds. As listed in Table 4, it is found out that the interatomic distance for the first shell increase slightly since Sn atom are substituted for Fe atom, and therefore that of Fe-Fe/Fe-Sn bond corresponding to unit cell parameter increase. Consequently, the displacement of Sn ion with larger ionic radius than that of Fe ion into perovskite B sites results in an increase of unit cell volume.

For the Fe-Sn scattering path, interatomic distance of Sn-O bond could be determined with the difference between the average interatomic distance for the first shell and the Fe-Sn interatomic distance since the atomic array is Fe-O-Sn. While the average interatomic distances for the first shell are 0.1967 and 0.1972 nm for $BaFe_{0.75}Sn_{0.25}O_{2.65}$ and $BaFe_{50}Sn_{0.50}O_{2.76}$ compounds, the interatomic distances of Sn-O bond are 0.2097 and 0.2134 nm, respectively. The result shows the Fe-O bond has more covalent character than $Sn^{4+}$-O bond with $4d^{10}$ state. Moreover, the oxygen atom are relatively more shifted to Fe atom in the $BaFe_{50}Sn_{0.50}O_{2.76}$ compound than in $BaFe_{0.75}Sn_{0.25}O_{2.65}$, which shows that the bond covalency of Fe-O increase with substitution amount of Sn ions. It is in a good agreement with XANES study in which the 1s→3d quadrupole transition has been shifted to higher energy.

**Table 4.** Structural parameters from EXAFS data analysis for the $BaFe_{0.75}Sn_{0.25}O_{2.65}$ and $BaFe_{0.50}Sn_{0.50}O_{2.76}$ compounds

| Compound | Path | Structural parameters from EXAFS | | | | | |
|---|---|---|---|---|---|---|---|
| | | N | $S_o^2$ | $\Delta E_o$ (eV) | R (nm) | | $\sigma^2$ ($\times 10^{-5}$ nm$^2$) |
| $BaFe_{0.75}Sn_{0.25}O_{2.65}$ | O | 4 | 0.85 | 0.3 | 0.188(2) | | 4.66 |
| | O | 6 | | -0.7 | 0.205(1) | | 5.01 |
| | Sr | 8 | | 1.2 | 0.337(9) | | 2.10 |
| | Fe | 4.5 | | 1.3 | 0.391(7) | | 2.89 |
| | Sn | 2.5 | | -2.1 | 0.406(4) | 0.4093* | 2.41 |
| $BaFe_{0.50}Sn_{0.50}O_{2.76}$ | O | 4 | 0.85 | 0.7 | 0.190(2) | | 6.24 |
| | O | 6 | | | 0.204(1) | | 6.71 |
| | Sr | 8 | | 0.9 | 0.343(1) | | 2.88 |
| | Fe | 3 | | 0.7 | 0.396(2) | | 3.99 |
| | Sn | 3 | | -1.3 | 0.410(6) | 0.4098* | 3.31 |

*The values of unit cell parameter from XRD study corresponding to the average value between Fe-Fe and Fe-Sn interatomic distances.

**Acknowledgment.** The present study was supported by a Yonsei University Research Grant for 1995 and also by the Basic Science Research Institute Program, Minisrty of Education of Korea, 1995, Project No. BSRI-95-3424. We are grateful to professor M. Normura, professor H. Terauchi, and Dr. K. Sakaue for their helps on the XAFS measurement in Japan.

## References

1. Eom, C. B.; Cava, R. J.; Fleming, R. M.; Philips, J. M.; van Dover, R. B.; Marshall, J. H.; Hsu, J. W. P.; Krajewski, J. J.; Peck, W. F. *Nature* **1992**, *258*, 1766.
2. Kim, M. G.; Ryu, K. H.; Yo, C. H. *J. Solid State Chem.* **1996**, *123*, 161.
3. Roh, K. S.; Kim, M. G.; Ryu, K. S.; Yo, C. H. *Solid State Commm.* **1996**, *100*, 565.
4. Lichtenberg, F.; Catana, A.; Mannhart, J.; Schlom, D. G. *Appl. Phys. Lett.* **1992**, *60*, 1138.
5. Kim, M. G.; Im, Y. S.; Oh, Y. J.; Kim, K. H.; Yo, C. H. *Physica B* **1997**, *229*, 338.
6. Vaclav, O. K.; Robert, W. F. *Phys. Rev. B* **1976**, *13*, 3268.
7. Bianconi, A. *Phys. Rev. B* **1982**, *26*, 2741.
8. Grunes, L. A. *Phys. Rev. B* **1983**, *27*, 2111.
9. Akesson, R.; Persson, L.; Sandstrom, M.; Wahlgren, U. *Inorg. Chem.* **1994**, *33*, 3715.
10. Jiang, T.; Ellis, D. E. *J. Mater. Res.* **1996**, *11*, 2242.
11. Calas, G.; Petiau, *J. Solid State Commun.* **1983**, *48*, 625.
12. Roe, A. L.; Schneider, D. J.; Mayer, R. J.; Pyrz, J. W.; Widom, J.; Que, L. *J. Am. Chem. Soc.* **1984**, *106*, 1676.
13. Cartier, C.; Momenteau, M.; Dartagy, E.; Fortaine, A.;

Tourillon, G.; Michalowicz, A.; Verdaguer, M. *J. Chem. Soc., Dalton Trans.* **1992**, 609.
14. Shiro, Y.; Sato, F.; Suzuki, T.; Iizuka, T.; Matsushita, T.; Oyanagi, H. *J. Am. Chem. Soc.* **1990**, *112*, 2921.
15. Randall, C. R.; Shu, L.; Chiou, Y. M.; Hagen, K. S.; Ito, M.; Kitajima, N.; Lachicotte, R. J.; Zang, Y.; Que, L. *Inorg. Chem.* **1995**, *34*, 1036.
16. Bair, R. A.; Goddard, W. *Phys. Rev. B* **1980**, *22*, 2767.
17. Fronzoni, G.; Decleva, P.; Lisini, A. *Chem. Phys.* **1993**, *174*, 57.
18. Rehr, J. J.; Mustre de Leon, J. ; Zabinsky, S. I.; Albers, R. C. *J. Am. Chem. Soc.* **1991**, *113*, 5135.
19. O'Day, P. A.; Rehr, J. J.; Zabinsky, S. I.; Brown, G. E. *J. Am. Chem. Soc.* **1994**, *116*, 2938.
20. Li, G. G.; Bridges, F.; Booth, C. H. *Phys. Rev. B* **1995**, *52*, 6332.
21. Teo, B. K. *EXAFS: Basic Principles and Data Analysis*; Springer-Verlag: Berline, 1986; pp 21-182.
22. Stern, E. A. *X-ray Absorption: Principles, Applications, Techniques of EXAFS, SEXAFS and XANES*; Koningsberger, D. C.; Prins, R., Eds.; Wiley: New York, 1988; pp 3-51.

# The Effect of Alkali Metal Ions on Nucleophilic Substitution Reactions of Alkali Metal Ethoxides with S-p-nitrophenyl 2-thiofuroate and 2-Thiophenethiocarboxylate in Absolute Ethanol

**Ik-Hwan Um*, Yoon-Jung Lee, Jung-Hyun Nahm, and Dong-Sook Kwon**

*Department of Chemistry, Ewha Womans University, Seoul 120-750, Korea*
*Received April 7, 1997*

Rate constants have been measured spectrophotometrically for the reactions of alkali metal ethoxides (EtOM) with *S*-p-nitrophenyl 2-thiofuroate (**1b**) and 2-thiophenethiocarboxylate (**2b**) in absolute ethanol at 25.0±0.1 °C. **1b** is observed to be more reactive than **2b** toward all the EtOM studied. The reactivity of EtOM is in the order EtOK>EtONa>EtO >EtOLi for both substrates, indicating that $K^+$ and $Na^+$ behave as a catalyst while $Li^+$ acts as an inhibitor in the present system. Equilibrium association constants of alkali metal ions with the transition state ($K_a^{TS}$) have been calculated from the known equilibrium association constants of alkali metal ion with ethoxide ion ($K_a$) and the rate constants for the reactions of EtOM with **1b** and **2b**. The catalytic effect ($K_a^{TS}/K_a$) is larger for the reaction of **1b** than **2b**, and decreases with decreasing the size of the alkali metal ions. Formation of 5-membered chelation at the transition state appears to be responsible for the catalytic effect.

## Introduction

The catalytic effect of metal ions on reactions of various types of esters with bases has been intensively studied.[1-3] However, most studies have been limited to divalent metal ions such as $Mg^{2+}$, $Zn^{2+}$, $Cu^{2+}$... etc.[4,5] Since Lewis acidity of monovalent alkali metal ions is much weaker than that of divalent cations, the effect of alkali metal ions on acyl-transfer reactions has not attracted much attention. Only recently Buncel,[6,7] Suh,[8] Modro[9] and our group[10] have initiated to investigate the effect of alkali metal ions on acyl-transfer reactions.

Buncel *et al.* found significant catalytic effect of alkali metal ions on the reaction of p-nitrophenyl diphenylphosphinate (PNPDPP) with alkali metal ethoxides (EtOM) in absolute ethanol, and the catalytic effect increases with increasing charge density of alkali metal ions, *e.g.* $K^+<Na^+<Li^+$.[6] On the contrary, the catalytic effect was observed to be in the order $K^+>Na^+>Li^+$ for the corresponding reaction of p-nitrophenyl benzenesulfonate.[7] However, alkali metal ions were found to exhibit inhibitory effect for the reaction of PNPDPP with alkali metal aryloxides (ArOM) in absolute ethanol,[10a] but little effect for the reaction of p-nitrophenyl benzoate (PNPB) with EtOM in absolute ethanol.[10b] These results suggest that the effect of $M^+$ ions (as catalyst or inhibitor) is dependent on substrates (phosphorus, sulfur and carbon centered esters) as well as on nucleophiles (EtO and $ArO^-$).

Recently, we found alkali metal ions show significant effect for the reaction of p-nitrophenyl 2-furoate (**1a**) and 2-thiophenecarboxylate (**2a**) with EtOM in absolute ethanol.[10c,d] Now we have extended our study to the reaction of alkali metal ethoxides (EtOM) with *S*-p-nitrophenyl 2-thiofuroate (**1b**) and 2-thiophenethiocarboxylate (**2b**) in order to investigate the effect of the replaced O atom by S atom in the ring of the acid moiety (**1**→**2**) as well as in the ether-like C-O-C bond (**a**→**b**).

## Experimental

**Materials.** *S*-p-nitrophenyl 2-thiofuroate (**1b**, mp 134-135 °C) and 2-thiophenethiocarboxylate (**2b**, mp 147-150 °C) were easily prepared from the reactions of p-nitrothiophenol with 2-furoyl chloride and 2-thiophenecarboxyl chloride, respectively, in the presence of triethylamine in methylene chloride.[10c,d] Their purity was checked by means of melting points and spectral data such as IR and $^1H$ NMR characteristics. Absolute ethanol was prepared by the method des-